Comparing the mechanism of water condensation and evaporation in glassy aerosol

David L. Bones[a], Jonathan P. Reid[a,1], Daniel M. Lienhard[b], and Ulrich K. Krieger[b]

[a]School of Chemistry, University of Bristol, Cantock's Close, BS8 1TS Bristol, United Kingdom; and [b]Institute for Atmospheric and Climate Science, ETH Zürich, Rämistrasse 101, 8092 Zürich, Switzerland

Edited by Mark H. Thiemens, University of California San Diego, La Jolla, CA, and approved June 12, 2012 (received for review January 20, 2012)

Atmospheric models generally assume that aerosol particles are in equilibrium with the surrounding gas phase. However, recent observations that secondary organic aerosols can exist in a glassy state have highlighted the need to more fully understand the kinetic limitations that may control water partitioning in ambient particles. Here, we explore the influence of slow water diffusion in the condensed aerosol phase on the rates of both condensation and evaporation, demonstrating that significant inhibition in mass transfer occurs for ultraviscous aerosol, not just for glassy aerosol. Using coarse mode (3–4 um radius) ternary sucrose/sodium chloride/aqueous droplets as a proxy for multicomponent ambient aerosol, we demonstrate that the timescale for particle equilibration correlates with bulk viscosity and can be $\gg 10^3$ s. Extrapolation of these timescales to particle sizes in the accumulation mode (e.g., approximately 100 nm) by applying the Stokes-Einstein equation suggests that the kinetic limitations imposed on mass transfer of water by slow bulk phase diffusion must be more fully investigated for atmospheric aerosol. Measurements have been made on particles covering a range in dynamic viscosity from <0.1 to $>10^{13}$ Pa s. We also retrieve the radial inhomogeneities apparent in particle composition during condensation and evaporation and contrast the dynamics of slow dissolution of a viscous core into a labile shell during condensation with the slow percolation of water during evaporation through a more homogeneous viscous particle bulk.

water uptake | whispering gallery modes | Raman spectroscopy | optical tweezers | viscous aerosol

Atmospheric aerosol particles are typically complex mixtures of organic and inorganic species with correspondingly complex equilibria and temporal responses to changes in humidity. Secondary organic aerosols (SOA) continue to receive a great deal of attention due to their impact on radiative forcing, mainly through the indirect effect (1). Ambient aerosol typically contains a significant organic fraction, arising from the oxidation of volatile organic compounds (2). SOA has been largely thought of as existing as a liquid phase, or as a combination of a solid phase within a liquid droplet, but the reality is likely to be far more nuanced. Recently, Virtanen et al. demonstrated that ambient SOA particles can have similar mechanical properties to crystalline $(NH_4)_2SO_4$ particles at 10–20% RH but exist as amorphous glasses to low relative humidity (RH) rather than forming crystalline phases (3). This picture is consistent with the conclusions of Mikhailov et al. (4) and Zobrist et al. (5), who suggested that the existence of glassy states may have profound consequences for the properties of atmospheric aerosol particles, particularly at low temperatures.

The term *glassy* refers to an amorphous, highly viscous state with a dynamic viscosity (η) of greater than 1×10^{12} Pa s and the mechanical properties of a solid (6). In thermodynamic terms, a glass is in a nonergodic metastable state, unable to rearrange to the lowest energy state (5, 7, 8). In this kinetically arrested form, it can be expected that water transport to and from the particle during condensation and evaporation is likely to be inhibited by diffusion and mixing within the particle bulk. Kinetic inhibition of homogeneous crystallization and water transport could affect the potential of SOA to act as ice nuclei (IN) or cloud condensation nuclei (CCN) and, in turn, influence the formation, number and properties of cloud droplets (5, 7, 9). There have been also indications that glassy aerosol could serve as heterogeneous ice nuclei, again influencing the properties of ice clouds (10). Further, not only can kinetic inhibition be expected for water transport, but for the transport of reactive species into the particle, the resulting rate of heterogeneous chemistry and the eventual evaporation of volatile and semi-volatile organic components into the gas phase. Shiraiwa et al. investigated the effect of viscosity on atmospheric aging directly, estimating that oxidation of organic compounds embedded within atmospheric particles at moderate RH can take place on a time scale of hours (11). Glassy aerosol can then act as a reservoir of otherwise reactive or volatile compounds, effectively trapping them in a glassy matrix (12, 13).

In previous work, we explored the kinetic limitations on water transport for single component sucrose particles that were exposed to evaporation and condensation steps (14, 15). Although sucrose may not be considered to be representative of SOA components in either functionality or O:C ratio, Koop et al. have concluded that the thermal glass transition temperature depends strongly on molecular mass and not strongly on the O:C ratio or functionality (8). Further, the highly oxidized organic acids that are a significant component of SOA have been shown to be of a similar viscosity to sucrose under atmospherically relevant conditions (5). Thus, we suggest that the ternary aqueous/sucrose/NaCl particles studied here are an excellent proxy system for study given that reliable thermodynamic and viscosity data have been published over a wide range of water activities and for varying compositions (16, 17). In this publication, we first explore the limitations of water transport in ternary aerosol particles, 3 to 4 μm in radius, consisting of both organic and inorganic components. In particular, we map out the relationship between the time response of water partitioning and the bulk viscosity, using a range of ternary sucrose/NaCl solutions. By varying the dry mass fraction of NaCl, the mole fraction of water at a given RH can be tuned and the viscosity of the particle can be varied, allowing access to dynamic viscosities over a broad range (<0.1 to $>10^{13}$ Pa s) expected to be of relevance to atmospheric aerosol. Finally, the gradients in water activity within a particle established during water transport are resolved through light scattering measurements, allowing us for the first time to directly compare and contrast the mechanisms of water transport during evaporation and condensation.

Results

Response Times for Water Transport in Ternary Mixtures. Changes in size of binary aqueous sucrose particles during evaporation or

Author contributions: D.L.B., J.P.R., and U.K.K. designed research; D.L.B. and D.M.L. performed research; D.L.B. and D.M.L. contributed new reagents/analytic tools; D.L.B. and D.M.L. analyzed data; and D.L.B., J.P.R., and U.K.K. wrote the paper.

The authors declare no conflict of interest.

This article is a PNAS Direct Submission.

[1]To whom correspondence should be addressed. E-mail: j.p.reid@bristol.ac.uk.

This article contains supporting information online at www.pnas.org/lookup/suppl/doi:10.1073/pnas.1200691109/-/DCSupplemental.

condensation of water have been shown to be dramatically hindered at low RH, with the timescales for particles to reach equilibrium exceeding 10,000 s, for both increasing and decreasing RH regimes (14, 15). The particles do not crystallize; they remain spherical and exhibit smooth growth curves with continuous water uptake/loss. Here, we explore the time response of ternary particles of sucrose/sodium chloride/water at 293 K between many pairs of initial and final RH values. Varying the molar ratio of sucrose to sodium chloride allows measurements of water transport over a wide range of bulk solution viscosities. Ternary solutions are nebulized and trapped in a single-beam gradient force optical trap (optical tweezers) (18) and the kinetics of water transport quantified from an exponential fit to the time response in particle size immediately following a step change in RH. Typical size changes are of the order of hundreds of nanometers for particles 3–4 μm in radius and occur over timescales from <10 s to >10,000 s. Although the size response does not strictly follow first-order kinetics, with the loss of water slowing considerably as the particle becomes more viscous and approaches the final state, this simple phenomenological approach is chosen as it provides a convenient way of quantifying and comparing rates of evaporation/condensation at early times during the time period that most of the size change occurs. For many of the cases where the kinetics of mass transfer in glassy aerosol must be understood (e.g., in the atmosphere) it is most important to quantify the inhibition in rate during this early part of the mass transfer process, during which most of the size change occurs, rather than the very slow but small changes in size that occur over a longer period of time. All response times reported are half-times, the time taken for the size of the particle to reach the halfway point between its initial size and final equilibrium size.

The time response in size does not just depend on the initial RH, but can also depend on the magnitude of the RH step. For this reason, we have mapped the response of particles between a large number of initial and final RH values. In Fig. 1*A*, each point represents a measurement between an initial and final RH for sucrose particles: the points in the lower right corner of the plot correspond to steps in decreasing RH (evaporation of water), and points in the upper left corner correspond to upward steps (condensation of water). The color denotes the ratio of the half-time of the size response to the half-time of the downstream RH probe response (log scale, see *Methods* section for details of RH probes). For transitions within the glassy regime [for RH <25% (5)], the response time is typically two orders of magnitude longer than for a particle at higher RH. It is clear that inhibition of mass transfer occurs not only below the glass transition, but also above, as is also evident from Fig. 1*B*. As water activity decreases with increasing solute concentration, the bulk of a particle becomes increasingly viscous, with reduced diffusion coefficients and slower water transport. Even at an initial RH of 50%, the slowing of the mass transfer rate is sufficiently pronounced to observe a kinetic limitation on evaporation even though the particle is a solution droplet. Ternary mixtures of sucrose and sodium chloride also show pronounced inhibition of water transport. Similar RH maps for the ternary systems are included in the *SI Text* (Figs. S1–S3) for three different molar ratios for the two solutes.

Correlation of Response Time and Particle Bulk Viscosity. For each ternary mixture of sucrose, sodium chloride, and water, we use the parameterization of Chenlo (19) to calculate the dependence of the dynamic viscosity (Pa s) on water activity, providing the best currently available method for estimating the viscosity for this system. The Aerosol Diameter Dependent Equilibrium Model (ADDEM) (20) is used to estimate solute molality and solution density as a function of RH. ADDEM assumes a simple additive relationship for the water activity of ternary organic-inorganic mixtures and a UNIFAC parameterization for activity coefficients for sucrose; that is, the water associated with the mixture is simply

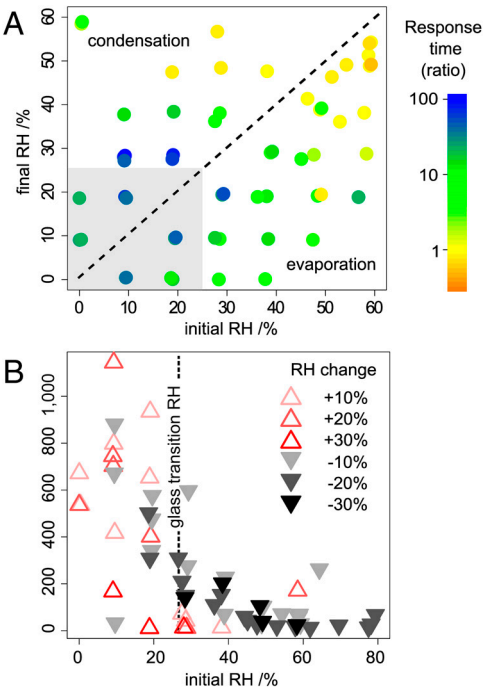

Fig. 1. (*A*) Ratio (logarithmic scale) of half-time for response in size of sucrose particle to half-time for RH probe response, mapped over range in initial and final RHs. The grey shaded area represents RH values below the glass transition. (*B*) Half-times (in seconds) between initial and final RH values.

the sum of the water associated with the organic and inorganic components separately, and no account is taken of nonideal interactions. The viscosity increases dramatically with decrease in water activity below about 0.4 for all of the ternary mixtures studied (Fig. S4). An examination of the contributions to the viscosity from the organic and inorganic components indicates that most of the variation in viscosity with increasing mole fraction of sodium chloride is due to dilution of the sucrose component by the extra water taken up by the sodium chloride component. A similar trend is expected for most inorganic components in inorganic/organic ternary mixtures. It must be noted that the parameterization of Chenlo only extends to molalities of 4.5 mol kg^{-1} for both sucrose and sodium chloride, the measurements being limited by the solubility of sodium chloride. As noted previously (15), we justify our use of this parameterization by noting that the trend in viscosity at low RH agrees with the model of He et al. (17). At the upper RH limit, the viscosities of all of the mixtures converge to the viscosity of water (1×10^{-3} Pa s).

The dependence of the measured response time on the predicted particle viscosity is shown in Fig. 2, for both condensation and evaporation, and for binary and ternary aerosol. The grey shaded area indicates the spread in timescales at the 1σ level when the data are averaged over narrow viscosity bins. At a first glance, this appears considerably narrower than the spread in the data, but reflects the large number of points that are broadly consistent. At any one viscosity, there can still be outliers, which is attributed to the unique conditioning experienced by each particle for a unique RH history, particularly the "waiting" time when below the glass transition (21). Future work will investigate this effect in greater detail. The viscosity is taken as the value at a water activity corresponding to the midpoint of the step in RH. For continuum mass transport limited by diffusion in the gas phase, the water activity at the droplet surface at the midpoint of the change corresponds to a water partial pressure gradient that has dropped to half of the starting value. Thus, in the dilute/high RH limit at low viscosities, the half-times are equivalent for eva-

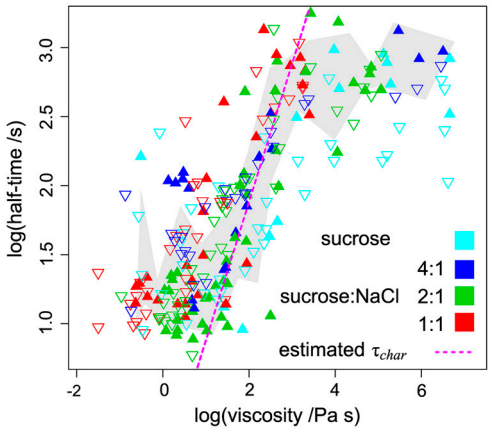

Fig. 2. Correlation of half-times for response of binary and ternary droplets with bulk viscosity (log scales) for steps in RH (open triangles, decrease in RH; filled triangles, increase in RH). The calculated characteristic time (τ_{char}), based on the Stokes-Einstein equation, is also plotted as a function of viscosity (pink line). The grey shaded region represents an estimate of experimental uncertainty about the mean values.

poration and condensation, since mass transport within the particle is rapid and the equilibration is governed by the change in partial pressure gradient. The gradient has the same magnitude for the evaporation and condensation cases when the water activity is changed between consistent upper and lower limits.

It should be noted that the time required for the RH change is of the order of 10 s in our experiment (22). Thus, we are not reliably able to measure timescales for mass transport that occur over a shorter time (i.e., for viscosities less than approximately 1 Pa s). Similarly, at viscosities above 10^4 Pa s, the timescale measurements should be interpreted with caution, with likely errors incurred in both the viscosity and time constant estimates. Given that the high viscosity measurements require a considerable extrapolation of the viscosity data, it is likely that the viscosity estimates could be in error by orders of magnitude (19). In addition, fitting a single exponential decay to the size response represents a simplification of the actual process, particularly under very dry/high viscosity conditions. The reported half times, although giving some indication of the timescale for the most significant part of the size change, are not expected to provide a good description for any event where the viscosity changes significantly and where the particle becomes ultraviscous approaching the glass transition. Thus, only measurements over the viscosity range 1 to 10^4 Pa s are considered in the following discussion. This viscosity range is highlighted in Fig. S4 and corresponds to water activities of between 0.10 and 0.35 for 1 : 1 NaCl/sucrose particles and 0.25 and 0.6 for pure sucrose particles.

For comparison with the experimental data over the viscosity range 1 to 10^4 Pa s, the characteristic half-time for diffusion into a spherical droplet ($\tau_{\frac{1}{2}}$) of radius r can be estimated from the expression (11, 23):

$$\tau_{\frac{1}{2}} = \frac{r^2}{\pi^2 D \cdot \ln(2)}$$

where the diffusion constant, D, is the binary diffusion constant and the factor of $\ln(2)$ converts the $1/e$ folding time into a half-time. To estimate D, we begin by naively assuming that the diffusion constant can be estimated from the viscosity of the particle bulk, even though the Stokes-Einstein equation is not expected to hold for concentrated solutions or in liquids near their glass transition temperature/RH (24). Indeed, for sucrose it has been reported that even at relatively dilute solute concentrations (e.g., between RH 30%–90%) the diffusion constant for water in sucrose, D_W, is decoupled from the diffusion constant of sucrose in water, D_{sucrose} (25). Pressing on, the Stokes-Einstein equation relates the diffusion constant to the dynamic viscosity:

$$D = \frac{k_B T}{6\pi a \nu}$$

where k_B is the Boltzmann constant, T is the temperature, a is the molecular radius (taken as 0.2 nm for water) and ν is the dynamic viscosity. The Stokes-Einstein equation assumes an inverse dependence on viscosity with a large (spherical) molecule moving in a continuum (26). For glassy or ultraviscous sucrose solution, we expect small molecules (H_2O) to percolate through a matrix of large hydrogen-bonded sucrose molecules (11). Despite all of these complexities, the predictions of the half-time from the Stokes-Einstein equation are found to be consistent with the experimental data over the viscosity range 1 to 10^4 Pa s, not only in agreement at the high RH (low viscosity) limit, but down to a water activity of 0.25 for both binary and ternary particles. Thus, the use of the Stokes-Einstein approach provides an empirically justified approach for *estimating* the equilibration timescale of the aerosol, even though the intricacies of the mechanism may not be fully congruent with the model.

Measurements of Radial Inhomogeneities in Water Activity. When a glassy or highly viscous particle is exposed to an increase in RH, the water activity at the surface of the particle is far from equilibrium and water condenses onto the particle surface. During dissolution of the viscous core, solute diffusion throughout the water layer is fast. Further dissolution of the core is accompanied by increased water condensation, maintaining equilibrium in the developing aqueous surface layer with the surrounding water vapor. Until the particle reaches equilibrium, the solute concentration in the aqueous layer will differ from the concentration within the core. In this section, we probe this gradient.

The resonance structure apparent in the Raman spectra of light scattered from the particle can be used to interrogate the internal structure of the particle. At wavelengths commensurate with whispering gallery modes (WGMs), the back-scattered Raman light is enhanced (27). Experimental evidence for the existence of a concentration gradient can be seen by the asynchronous shifts in resonant modes of different orders relative to each other (Fig. 3), atypical behavior when compared with what is expected when a homogeneous particle changes in size (Fig. S5*A*). This mode shift is clearest in the binary sucrose-water system, but has also been observed in the ternary systems and for other compounds. The internal electric field within the particle can be described by a summation of partial waves, with the weighting of one particular partial wave dominant when the particle circumference and wavelength match the resonant condition of a WGM.

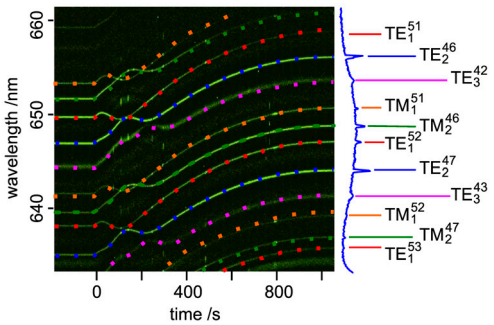

Fig. 3. Time response in resonance mode wavelengths as the size of the sucrose particle changes during water condensation following an increase in the RH from 20% to 40% at $t = 0$ s. Modes of different polarisation (TE, TM) move together while modes of different order ($l = 1$, $l = 2$, $l = 3$) shift asynchronously. The final spectrum is displayed vertically with the mode assignment indicated.

Thus, WGMs can be assigned a mode number (n) and a mode order (l), which describe the radial and angular variation of the light intensity within the particle (28). We use the notation Pol_l^n, where Pol refers to the polarization (TE or TM designates transverse electric and transverse magnetic respectively). The light intensity is concentrated near the particle surface to a depth of $\sim(r - r/m)$, where m is the refractive index. As l increases, the region with the highest light intensity occurs at a greater depth.

The condensation process described above might be expected to be consistent with a glassy core and a more dilute shell, with the refractive index of the core set by the drying process and corresponding to the lowest water activity achieved. As water is taken up by the particle, the shell increases in thickness and the core boundary retreats. The dissolution front passes sequentially through the maxima in light intensity of modes of increasing mode order. This is broadly consistent with the asynchronous changes in the wavelengths of the modes of different orders seen in Fig. 3, with the $l = 1$ modes moving in advance of the $l = 2$ and then the $l = 3$ modes. To more quantitatively assess the concentration gradient within the particle, Mie-Lorenz calculations are used to predict the position of the resonant modes for a particle with various radial concentration profiles. The particle can be modeled as a series of concentric shells, each with a distinct refractive index. We use the algorithm provided by Peña and Pal to compute the scattering coefficient for a layered particle (29), considering the specific case of a sucrose particle subjected to an abrupt increase in RH, from 20% to 40%. For the majority of calculations, 97 evenly spaced layers are used. A concentration profile is calculated at each time step (e.g., 5 seconds) which is then converted into a refractive index profile. The radial movement of the diffusion front is chosen to match the timescales of the experimentally observed mode shifts. The total amount of solute in the particle is fixed and the total radius is adjusted accordingly as the concentration profile changes.

When the simulation assumes a homogeneous concentration profile during water uptake, the modes move in concert (Fig. S5*A*). For simulations in which the concentration at the core and at the surface are different, irrespective of whether the radial concentration profile is a distinct step or smooth, asynchronous shifts in the $l = 1$ and $l = 2$ modes are found and qualitatively reproduce the trends seen experimentally (e.g., *SI Text*, Figs. S5 *B–D*). The relative shifts in modes of different polarization and order are shown in Fig. 4, from the measurements (Fig. 4*A*) and from a set of simulations that restrict the concentration profile to that of a core-shell morphology (Fig. 4*B* from Fig. S5*B*). The wavelength of one mode of one polarization and order is subtracted from the neighboring mode of opposite polarization or different mode order. The relative shifts are much more pronounced between modes of different order than between modes of different polarization. The core-shell simulations reproduce the observed relative mode shifts more closely than simulations with other concentration profiles, including both linear and sigmoidal gradients; this is consistent with expectations from the radial concentration profiles predicted from diffusion modeling (14).

The core size and shell thickness directly retrieved from fitting the spectra to a core-shell model are shown in Fig. 5 for the condensation process shown in Fig. 3. The core refractive index is taken as the refractive index at the lowest water activity following drying, and the shell refractive index is taken as that for a solution at equilibrium with the new gas phase relative humidity. Up to a shell thickness of 900 nm, the fit is excellent and the growth of the shell, hence the contraction of the core, is more or less linear. Above 900 nm, the WGMs are insensitive to the core and the droplet resembles a homogeneous aqueous sucrose droplet at a water activity of 0.4. The rate of dissolution is approximately half as fast as that estimated from the ETH diffusion model (14) (lower panel, Fig. 5). This is consistent with our previous work, which found that the measured time-response was

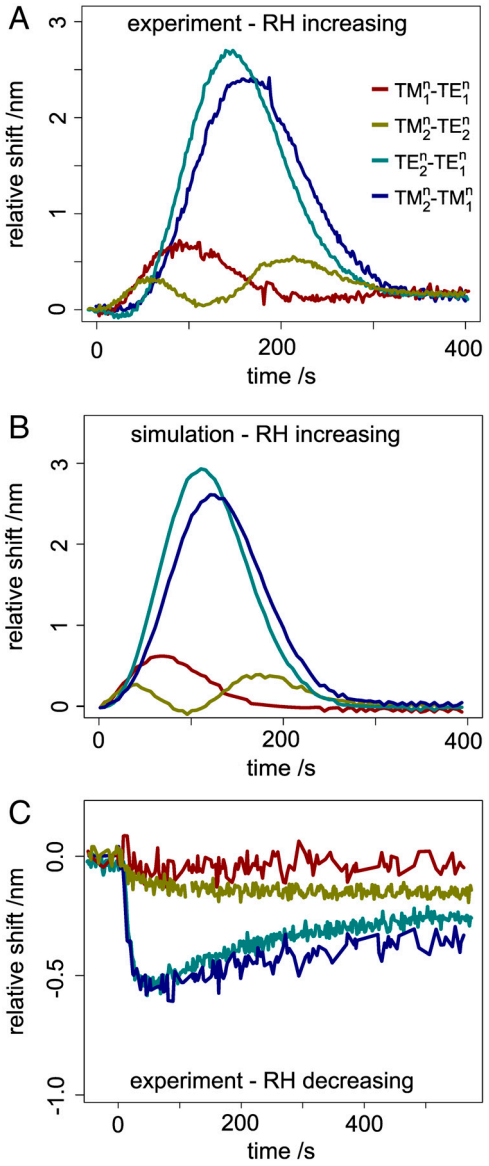

Fig. 4. Relative shifts in the wavelengths of resonance modes between the various polarizations and mode orders. (*A*) Experimental mode shifts recorded for a sucrose particle subjected to a rise in RH from 20% to 40% (at time = 0 s). (*B*) Simulated mode shifts under the same conditions for a droplet of core-shell morphology. (*C*) Relative mode shifts observed after the RH is decreased from 30% to 0%; i.e., the evaporation case. The mode shifts are more subtle than those observed when water condenses on the particle.

consistently slower than that expected from the diffusion model for sucrose aerosol (15), and with expected uncertainties in the diffusion constant of water at high solute concentrations (Fig. S6).

On evaporation, the relative shifts in modes of different order are much more subtle (Fig. 4*C* and Fig. S7). Either the concentration gradients established are very slight over a considerable depth or a very thin crust is established on the surface of the droplet. Over the propagation depth of the light (hundreds of nanometers), the observations are consistent with a particle of almost homogeneous refractive index. Given the sequential small steps in RH through which the particle has passed, a considerable degree of homogeneity in composition is to be expected. However, the transport of water becomes slow and the size change is kinetically limited by the slow release/percolation of water from throughout the droplet bulk.

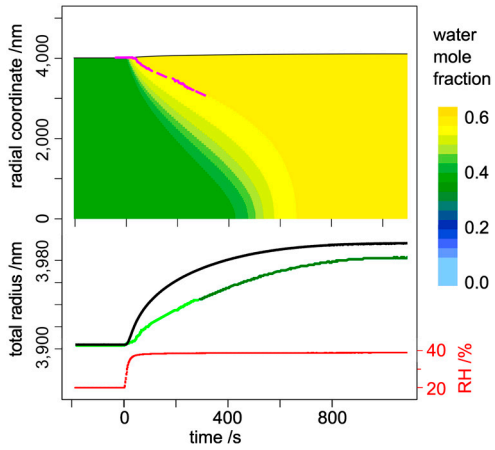

Fig. 5. Change in morphology for a sucrose particle exposed to an RH increase from 20% to 40% RH. *Top*: Measured change in core radius (pink) overlaid on the concentration profile from the ETH diffusion model. The model shows a marked boundary in water mole fraction, approximating to a core-shell structure. *Lower*: The total radius from the experiment as estimated assuming a core-shell profile (up until 300 s, light green) and a homogeneous profile at a water activity of 0.4 (after 300 s, dark green). Predictions for total radius from the ETH diffusion model (black) and the experimental trend in RH (red) are also shown. The model predicts a more rapid dissolution of the core and penetration of the shell than is measured.

To summarize, in these measurements we resolve differences in the mechanism of water transport during uptake and release of water. On condensation, an aqueous shell forms quickly as the RH increases, maintaining the surface of the particle at the water activity corresponding to the ambient RH and establishing a particle of core-shell structure. The dissolution of sucrose and condensation of water then proceed in concert and the initial size response of the particle is governed by the rate of diffusion of the solute in the aqueous phase. Evaporation, by contrast, is instead limited by the slow diffusion/percolation of water in a highly viscous bulk that is fairly uniform in composition.

Atmospheric Implications. Current models of atmospheric aerosol assume that the properties of the aerosol (e.g., size distribution, hygroscopicity) are governed by equilibrium thermodynamics. The presence of glassy and/or highly viscous aerosol in the atmosphere highlights the importance of quantifying the rates of change of these properties. Given the validity reported here of using the ADDEM model for treating the equilibrium state, the Chenlo parameterization for estimating viscosity and the Stokes-Einstein equation for diffusivity for mixed component aerosol, we can predict the time response of highly viscous particles within the accumulation mode, as reported in Fig. 6*A* and Fig. S8. The timescales shown are for a ±20% change in RH with the midpoint at the RH change indicated. It should be noted that we show timescale estimates for aerosol particles that lie outside of the viscosity range that we can reliably probe, 1 to 10^4 Pa s, and some caution must be exercised in interpreting predictions outside this range. Further, any possible influence of surface curvature (i.e., the Kelvin term) has been neglected to provide these timescale estimates.

First, we can conclude that at ambient temperatures typical of HTDMA (Hygroscopicity Tandem Differential Mobility Analyzer) experiments, it may be only crucial to consider the response time for particles when drying aerosols dominated by an organic component to below 10% RH, the first stage in a hygroscopic growth measurement. An HTDMA system consists of two differential mobility analysers (DMA). The first DMA selects a monodisperse aerosol distribution which is then exposed to a particular relative humidity, allowing timescales on the order of 10 s for equilibration (e.g., refs. 30 and 31). The second DMA then sizes

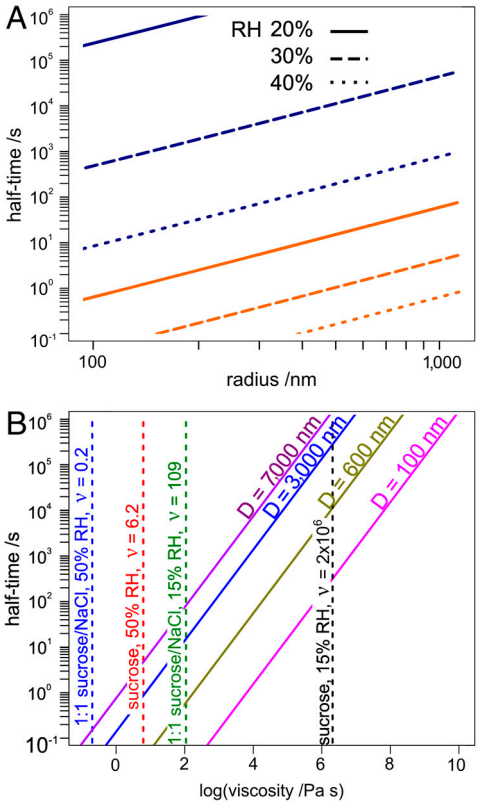

Fig. 6. (*A*) Predicted dependence of half-time on particle size for accumulation mode particles at 273 K. Orange: 1:1 sucrose:NaCl, Navy: pure sucrose. (*B*) Predictions of the half-time as a function of viscosity for particles of four diameters. Relevant viscosities of binary and ternary solutions used in this study at room temperature (293 K) are included for comparison (vertical lines).

the particles to determine their hygroscopicity. While the response time of mixed component particles is <10 s for all sizes for a change in RH between 10% and 30% at 293 K (Fig. S8, green line), the response time for pure component sucrose particles is ≫10 s for all particle sizes between 0.1 and 1 μm. In addition, these simulations suggest that the variability in time response between particles of different composition may be considerable—indeed, many orders of magnitude—leading to considerable ambiguity when interpreting measurements. It should be stressed that this variability in timescale with composition arises from the dependence of viscosity on composition, particularly the mass fraction of condensed phase water. Water acts as a plasticizer, as suggested by previous studies (8, 11). Thus, particles of very different composition may show the same time-response for water mass transport at wildly differing RHs because their viscosities (and water diffusion constants) are in fact the same.

In Fig. 6*B*, we show how the estimated timescale for the equilibration varies with viscosity for particles of different size. It should be remembered that the quoted timescale is for half the size change; the timescale for the particle to fully reach an equilibrium size will be considerably longer. The timescales for equilibration of particles of 600 and 100 nm diameter only become significant (>10 s) once the dynamic viscosity increases above 10^3 Pa s and 10^5 Pa s, respectively. Although these values are considerably lower than the dynamic viscosity of the glasses (>10^{13} Pa s) which have been observed in the atmosphere (3), the actual viscosity of atmospheric aerosol is highly uncertain, and it is not yet clear under what conditions these lower limits for viscosity will be surpassed and water transport inhibited (8). However, it is clear that the viscosity of atmospheric aerosol

spans a broad range from approximately 10^{-3} Pa s for dilute solution droplets to $>10^{13}$ Pa s for solid particles.

An improved understanding of the hygroscopicity and internal composition of organic aerosol will enable us to better predict the behavior of aerosol particles as IN and CCN. The correlation of response time with viscosity gives us a tool for estimating the rate of a kinetically hindered physical process such as water transport. Subsequent measurements must determine if the viscosity range over which the kinetic limitation of water transport is expected is relevant to atmospheric particles, which will be characterized by a considerably greater degree of chemical complexity and smaller particle size than studied here (8). While some chamber measurements suggest that kinetic limitations to water transport in SOA may exist (32), measurements on ambient samples are less conclusive (33). The response times for particles subjected to increasing RH and those subjected to decreasing RH are similar and can be modeled by the Stokes-Einstein treatment of diffusion. However, the observation of mode shifts for increases in RH is evidence for a different process occurring during water uptake. Immediately following an increase in RH (with initial RH below the glass transition RH), a core-shell structure appears and persists for hundreds of seconds. Such measurements give new insights into the properties of aerosol in an amorphous state.

Methods

The experimental setup has been described in depth previously (34). To summarize, an aqueous aerosol droplet 3–4 μm in radius is trapped in optical tweezers. Cavity-enhanced Raman scattering (CERS) spectra are collected by a CCD detector after dispersal of the Raman light in a Triax 550 spectrograph (Horiba Jobin-Yvon). The wavelengths of the Mie resonances in the spectra allow accurate sizing of the particles. In this way, we can monitor the size response to changes in RH. RH is measured by Honeywell capacitance probes, upstream and downstream of the trapping cell, and is varied by controlling the relative flow of saturated and dry streams of nitrogen. Remote control of the flow meters via a preprogrammed sequence allows for a systematic study of abrupt changes in relative humidity, both up and down. A typical downstream probe response is around 20 s. The solutions studied all had a dry mass fraction of sucrose of 0.85 or higher. Thus, the contribution from sucrose dominated the refractive index, and a previously obtained parameterization for the variation in refractive index with the concentration of binary sucrose (15) was sufficient to size all of the particles trapped.

ACKNOWLEDGMENTS. J.P.R. and D.L.B. acknowledge the EPSRC for funding through the support of a Leadership Fellowship awarded to J.P.R.. U.K.K. and D.M.L. acknowledge the ETH research Grant ETH-0210-1.

1. Pierce JR, et al. (2011) Quantification of the volatility of secondary organic compounds in ultrafine particles during nucleation events. *Atmos Chem Phys* 11:9019–9036.
2. Jimenez JL, et al. (2009) Evolution of organic aerosols in the atmosphere. *Science* 326:1525–1529.
3. Virtanen A, et al. (2010) An amorphous solid state of biogenic secondary organic aerosol particles. *Nature* 467:824–827.
4. Mikhailov E, Vlasenko S, Martin ST, Koop T, Pöschl U (2009) Amorphous and crystalline aerosol particles interacting with water vapor: conceptual framework and experimental evidence for restructuring, phase transitions and kinetic limitations. *Atmos Chem Phys* 9:9491–9522.
5. Zobrist B, Marcolli C, Pedernera DA, Koop T (2008) Do atmospheric aerosols form glasses? *Atmos Chem Phys* 8:5221–5244.
6. Angell CA (1995) Formation of glasses from liquids and biopolymers. *Science* 267:1924–1935.
7. Debenedetti PG, Stillinger FH (2001) Supercooled liquids and the glass transition. *Nature* 410:259–267.
8. Koop T, Bookhold J, Shiraiwa M, Poschl U (2011) Glass transition and phase state of organic compounds: Dependency on molecular properties and implications for secondary organic aerosols in the atmosphere. *Phys Chem Chem Phys* 13:19238–19255.
9. Murray BJ, Bertram AK (2008) Inhibition of solute crystallisation in aqueous H^+-NH_4^+-SO_4^{2-}-H_2O droplets. *Phys Chem Chem Phys* 10:3287–3301.
10. Murray BJ, et al. (2010) Heterogeneous nucleation of ice particles on glassy aerosols under cirrus conditions. *Nat Geosci* 3:233–237.
11. Shiraiwa M, Ammann M, Koop T, Pöschl U (2011) Gas uptake and chemical aging of semisolid organic aerosol particles. *Proc Natl Acad Sci USA* 108:11003–11008.
12. Vaden TD, Imre D, Beránek J, Shrivastava M, Zelenyuk A (2011) Evaporation kinetics and phase of laboratory and ambient secondary organic aerosol. *Proc Natl Acad Sci USA* 108:2190–2195.
13. Cappa CD, Wilson KR (2011) Evolution of organic aerosol mass spectra upon heating: Implications for OA phase and partitioning behavior. *Atmos Chem Phys* 11:1895–1911.
14. Zobrist B, et al. (2011) Ultra-slow water diffusion in aqueous sucrose glasses. *Phys Chem Chem Phys* 13:3514–3526.
15. Tong H-J, Reid JP, Bones DL, Luo BP, Krieger UK (2011) Measurements of the timescales for the mass transfer of water in glassy aerosol at low relative humidity and ambient temperature. *Atmos Chem Phys* 11:4739–4754.
16. Shalaev EY, Franks F, Echlin P (1996) Crystalline and amorphous phases in the ternary system water-sucrose-sodium chloride. *J Phys Chem* 100:1144–1152.
17. He X, Fowler A, Toner M (2006) Water activity and mobility in solutions of glycerol and small molecular weight sugars: Implication for cryo- and lyopreservation. *J Appl Phys* 100:074702.
18. Wills JB, Knox KJ, Reid JP (2009) Optical control and characterisation of aerosol. *Chem Phys Lett* 481:153–165.
19. Chenlo F, Moreira R, Pereira G, Ampudia A (2002) Viscosities of aqueous solutions of sucrose and sodium chloride of interest in osmotic dehydration processes. *J Food Eng* 54:347–352.
20. Topping DO, McFiggans GB, Coe H (2005) A curved multi-component aerosol hygroscopicity model framework: Part 2—including organic compounds. *Atmos Chem Phys* 5:1205–1222.
21. Amir A, Oreg Y, Imry Y (2012) On relaxations and aging of various glasses. *Proc Natl Acad Sci USA* 109:1850–1855.
22. Hargreaves G, et al. (2010) Measurements of the equilibrium size of supersaturated aqueous sodium chloride droplets at low relative humidity using aerosol optical tweezers and an electrodynamic balance. *J Phys Chem A* 114:1806–1815.
23. Seinfeld JH, Pandis SN (1998) *Atmospheric Chemistry and Physics: From Air Pollution to Climate Change* (John Wiley and Sons, Inc, New York), 1st Ed.
24. Champion D, Hervet H, Blond G, Meste ML, Simatos D (1997) Translational diffusion in sucrose solutions in the vicinity of their glass transition temperature. *J Phys Chem B* 101:10674–10679.
25. Molinero V, Çağin T, Goddard WA, III (2003) Sugar, water and free volume networks in concentrated sucrose solutions. *Chem Phys Lett* 377:469–474.
26. Poling BE, Prausnitz JM, O'Connell JP (2001) *The Properties of Gases and Liquids* (McGraw-Hill Companies, Inc, Boston), 5th Ed.
27. Reid JP, Meresman H, Mitchem L, Symes R (2007) Spectroscopic studies of the size and composition of single aerosol droplets. *Intl Rev Phys Chem* 26:139–192.
28. Symes R, Sayer RM, Reid JP (2004) Cavity enhanced droplet spectroscopy: Principles, perspectives and prospects. *Phys Chem Chem Phys* 6:474–487.
29. Peña O, Pal U (2009) Scattering of electromagnetic radiation by a multilayered sphere. *Comput Phys Commun* 180:2348–2354.
30. Zardini AA, et al. (2008) A combined particle trap/HTDMA hygroscopicity study of mixed inorganic/organic aerosol particles. *Atmos Chem Phys* 8:5589–5601.
31. Gysel M, et al. (2004) Hygroscopic properties of water-soluble matter and humic-like organics in atmospheric fine aerosol. *Atmos Chem Phys* 4:35–50.
32. Asa-Awuku A, Engelhart GJ, Lee BH, Pandis SN, Nenes A (2009) Relating CCN activity, volatility, and droplet growth kinetics of beta-caryophyllene secondary organic aerosol. *Atmos Chem Phys* 9:795–812.
33. Engelhart GJ, et al. (2011) Water content of aged aerosol. *Atmos Chem Phys* 11:911–920.
34. Mitchem L, Reid JP (2008) Optical manipulation and characterisation of aerosol particles using a single-beam gradient force optical trap. *Chem Soc Rev* 37:756–769.

Supporting Information

Bones et al. 10.1073/pnas.1200691109

SI Text

Modeling the Concentration Gradient as a Sigmoidal Function. In the case illustrated in Fig. S5*C*, the concentration gradient is modeled as a sigmoidal function. The surface and core concentrations were set to the experimental values, as for the linear gradient and core-shell cases. Between the radius and the core, the concentration was varied by the following equation:

$$c = \frac{c_{\text{core}} - c_{\text{surf}}}{1 + e^{(r+At)*\frac{5}{At}}} + c_{\text{surf}}$$

where c_{core} is the initial concentration in the core, and c_{surf} is the concentration at the surface of the particle, which will match the water activity of the gas phase. t is the time in seconds and r is the radial coordinate. A is a parameter based on the speed of the diffusion front.

Simulations of Changing Water Partitioning during Condensation. The amount of solute in the particle was kept constant by adjusting the radius, which was seen to grow as the water diffuses into the particle. The predicted mode shifts for the core-shell, sigmoidal, and linear concentration gradient models are similar, but the core-shell most closely reflects the internal concentration gradient predictions from the ETH diffusional model.

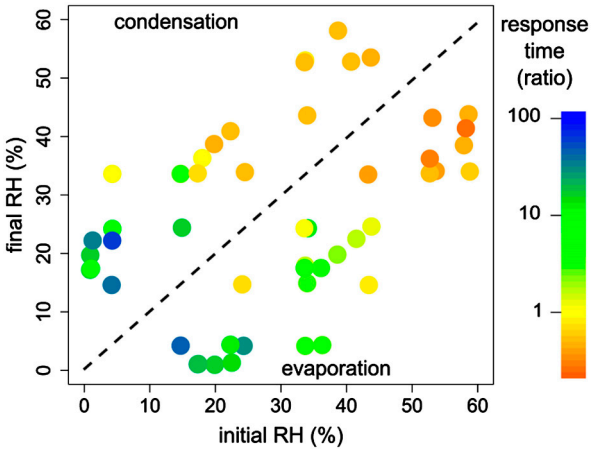

Fig. S1. Ratio (logarithmic scale) of half-time for response in size of particle to half-time for RH probe response, mapped over a wide range in initial and final RHs for ternary mixtures of sucrose/NaCl/water (1:1 sucrose:NaCl molar ratio).

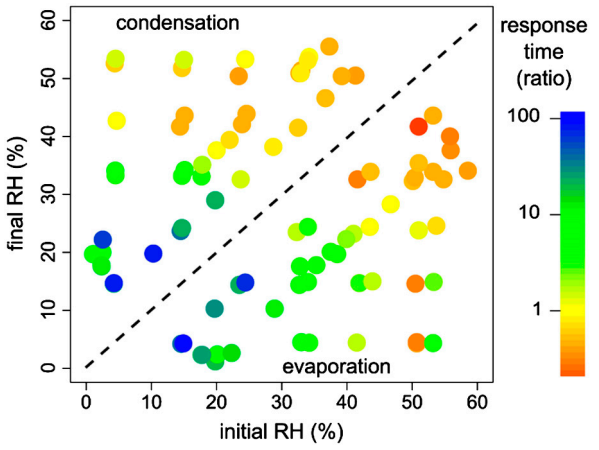

Fig. S2. Ratio (logarithmic scale) of half-time for response in size of particle to half-time for RH probe response, mapped over a wide range in initial and final RHs for ternary mixtures of sucrose/NaCl/water (2:1 sucrose:NaCl molar ratio).

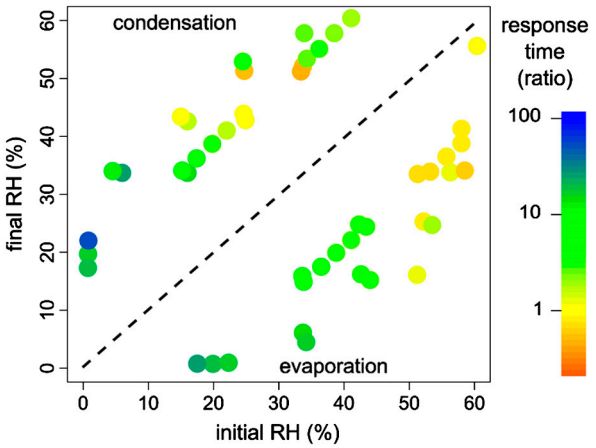

Fig. S3. Ratio (logarithmic scale) of half-time for response in size of particle to half-time for RH probe response, mapped over a wide range in initial and final RHs for ternary mixtures of sucrose/NaCl/water (4:1 sucrose:NaCl molar ratio).

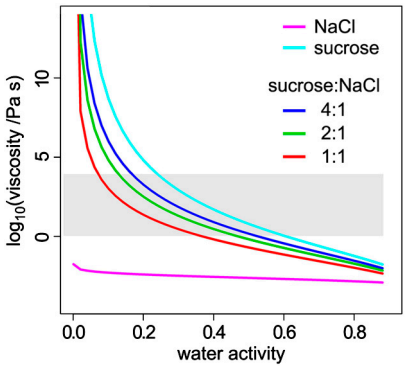

Fig. S4. Viscosity (as the base 10 log) as a function of water activity, calculated from ADDEM and the Chenlo parameterisation (1, 2). The grey shaded box indicates the viscosity range over which the correlation between half-time and viscosity is tested.

1 Topping DO, McFiggans GB, Coe H (2005) A curved multi-component aerosol hygroscopicity model framework: Part 2—including organic compounds. *Atmos Chem Phys* 5:1205–1222.
2 Chenlo F, Moreira R, Pereira G, Ampudia A (2002) Viscosities of aqueous solutions of sucrose and sodium chloride of interest in osmotic dehydration processes. *J Food Eng* 54:347–352.

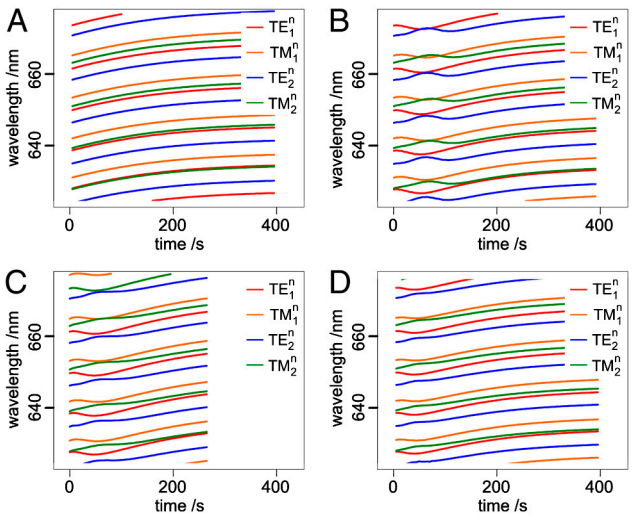

Fig. S5. Simulation of the changes in wavelengths of resonance modes following an increase in RH from 20% to 40% for a sucrose particle. Case *a*) assumes droplet growth retains a homogeneous composition. Case *b*) assumes droplet growth progresses by the deposition of an aqueous shell on a viscous sucrose core. Case *c*) assumes droplet growth progresses through the formation of a sigmoidal gradient in composition extending from the particle surface to the homogeneous core. Case *d*) assumes droplet growth progresses through the formation of a linear gradient in composition extending from the particle surface to the homogeneous core.

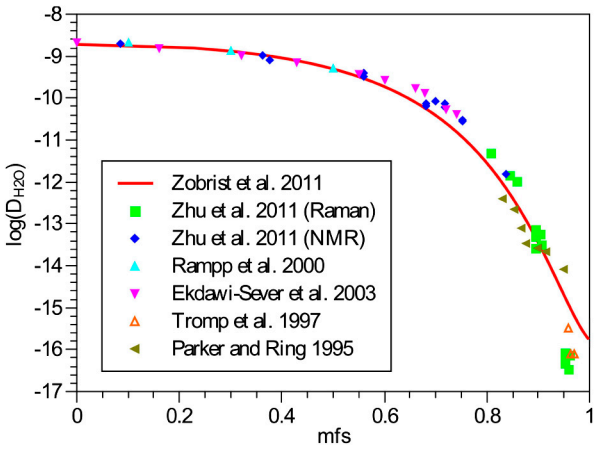

Fig. S6. Logarithm of the diffusion constant of water, D_{H_2O}, as a function of mass fraction of solute (mfs) at room temperature. Adapted from Zhu et al. (1) and references therein (2–5). The ETH diffusion model (6) matches the experimental data to within a factor of 2 around the relevant mfs (~0.9, which corresponds to a water activity of about 0.3).

1 Zhu L, et al. (2011) Water self-diffusion in glassy and liquid maltose measured by Raman microscopy and NMR. *J Phys Chem B* 115:5849–5855.
2 Ekdawi-Sever N, de Pablo JJ, Feick E, von Meerwall E (2003) Diffusion of sucrose and alpha,alpha-trehalose in aqueous solutions. *J Phys Chem A* 107:936–943.
3 Parker R, Ring SG (1995) Diffusion in maltose-water mixtures at temperatures close to the glass transition. *Carbohydr Res* 273:147–155.
4 Rampp M, Buttersack C, Ludemann HD (2000) C,T-dependence of the viscosity and the self-diffusion coefficients in some aqueous carbohydrate solutions. *Carbohydr Res* 328:561–572.
5 Tromp RH, Parker R, Ring SG (1997) Water diffusion in glasses of carbohydrates. *Carbohydr Res* 303:199–205.
6 Zobrist B, et al. (2011) Ultra-slow water diffusion in aqueous sucrose glasses. *Phys Chem Chem Phys* 13:3514–3526.

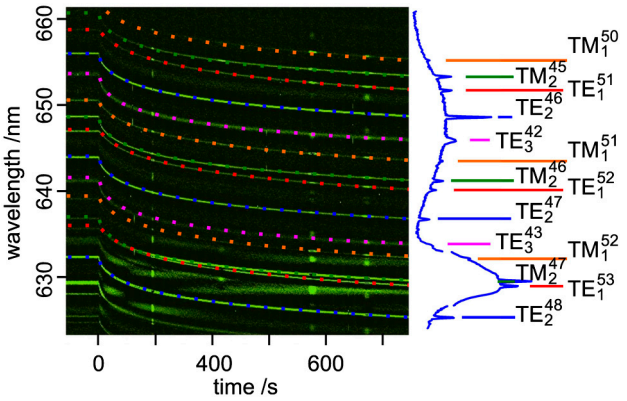

Fig. S7. Time response in resonance mode wavelengths as the size of the sucrose particle changes during water evaporation. The RH is decreased from 30 to 0% at $t = 0$ s. Modes of different polarisation (TE, TM) move together while modes of different order ($l = 1$, $l = 2$, $l = 3$) shift asynchronously, although to a lesser extent than in condensation (see Fig. 4). The final spectrum is displayed vertically with the mode assignment indicated.

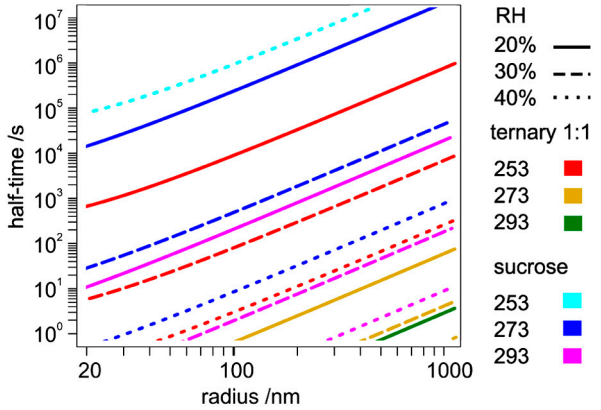

Fig. S8. Predicted dependence of half-time on particle size for accumulation mode particles, calculated using ADDEM, the Chenlo parameterisation and the Stokes-Einstein equation. This is analogous to Fig. 6*A*, but shows a broader range of RH changes and temperatures. The temperatures (in *K*) are indicated for the different color lines. All RH changes are ±20% about the RH indicated by the line type.